Mechanistic Model for Improved Performance of mRNA-LNPs Formulated Under Turbulent Mixing Conditions

Richard Mosesso [a], Katie Randall [a], Amita Vaidya [a,*], Jackie Tang [a], Trent Northen [a], Aurélie Deliot [b], Mengwei Sun [a], Rebecca Goldman [a], Adam Lyons [a], Lingyun Liu [a], Shrirang Karve [a], and Frank DeRosa [a]

Author Affiliations:

[a] mRNA Center of Excellence, Sanofi, 200 West St, Waltham MA 02451, USA

[b]VCDS Department, Sanofi Pasteur, 1541 Av. Marcel Mérieux, 69280, Marcy-L'Étoile, France

*** Corresponding Authors:**

Amita Vaidya

amita.vaidya@sanofi.com

L (inches)	L (m)	TFR ($mL \cdot min^{-1}$)	TFR ($m^3 \cdot s^{-1}$)	Cross Sectional Area (m^2)	Linear Velocity ($m \cdot s^{-1}$)	$^{*}\rho_{20\% EtOH}$ ($kg \cdot m^{-3}$)	$^{†}\mu_{20\% EtOH}$ ($kg \cdot m^{-1} \cdot s^{-1}$)	Re
0.125	0.003175	62.5	1.042E-06	7.917E-06	0.132	970.4	0.00173	234
0.125	0.003175	250	4.167E-06	7.917E-06	0.526	970.4	0.00173	937
0.09375	0.002381	312.5	5.208E-06	4.453E-06	1.169	970.4	0.00173	1562
0.0625	0.001588	312.5	5.208E-06	1.979E-06	2.631	970.4	0.00173	2343
0.0625	0.001588	625	1.042E-05	1.979E-06	5.263	970.4	0.00173	4686

*measured

†estimated

Supplemental Table 1. Calculations of Re for T-mixers and flow rates used in this study. L = T-mixer inner diameter, TFR = total flow rate, ρ = density, μ = viscosity (approximating dynamic viscosity ≈ bulk viscosity).

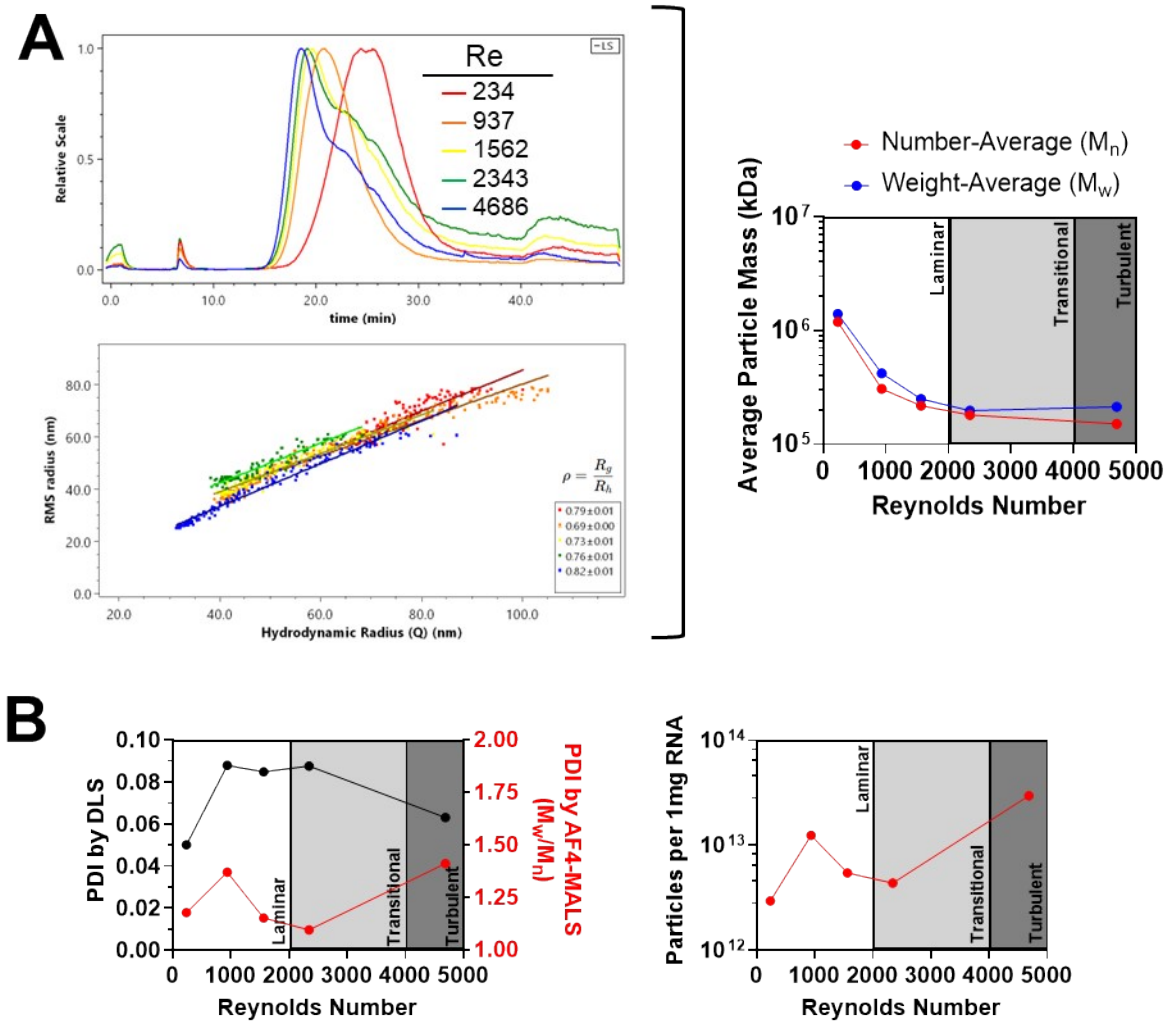

Supplemental Figure 1. Characterization of OF-02 LNPs by AF4-MALS-dRI-UV-DLS. (A) Raw traces, shape factor analysis, and average particle mass for LNPs made at different Re. (B) Comparison of PDI by DLS and AF4-MALS, and particle count per mRNA mass.

$f(x) = ax^3 + bx^2 + cx + d$ | $f(x)$ = Zeta potential (mV), x = pH

Re	a	b	c	d	R^2
234	-1.099	17.75	-97.43	191.2	0.98
937	-0.9128	14.75	-81.21	160.5	0.98
1562	-1.083	18.1	-101.7	199.5	0.99
2343	-1.172	19.38	-108.1	210.6	0.97
4686	-1.463	24.82	-140.5	272.1	0.99

Supplemental Table 2. Coefficients and R^2 values for trinomial fits of zeta potential measurements as a function of pH.

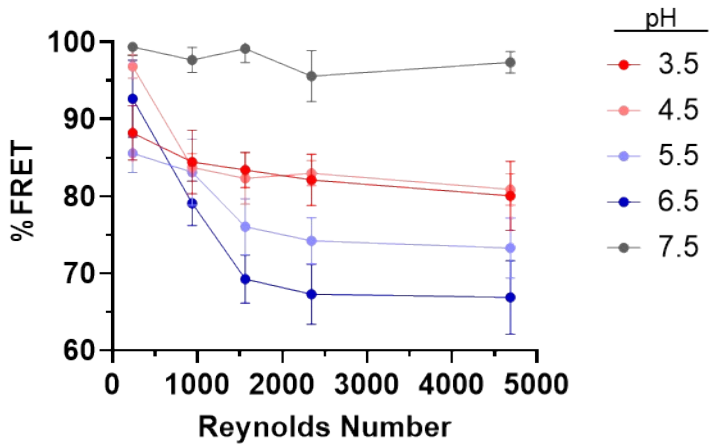

Supplemental Figure 2. Analysis of model endosome fusion with LNPs made at different Re by FRET. Intensity of the FRET signal decreases with increasing Re at pH < 7.5, although the effect of Re is less pronounced at pH < 6.5.

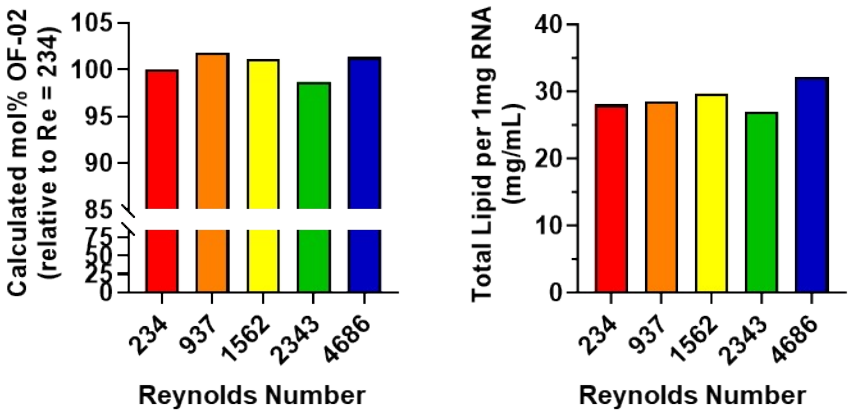

Supplemental Figure 3. UPLC-CAD analysis of OF-02 LNPs made at different Re. LNPs did not vary significantly in the relative mol% of OF-02 or the total lipid content per mass of mRNA.

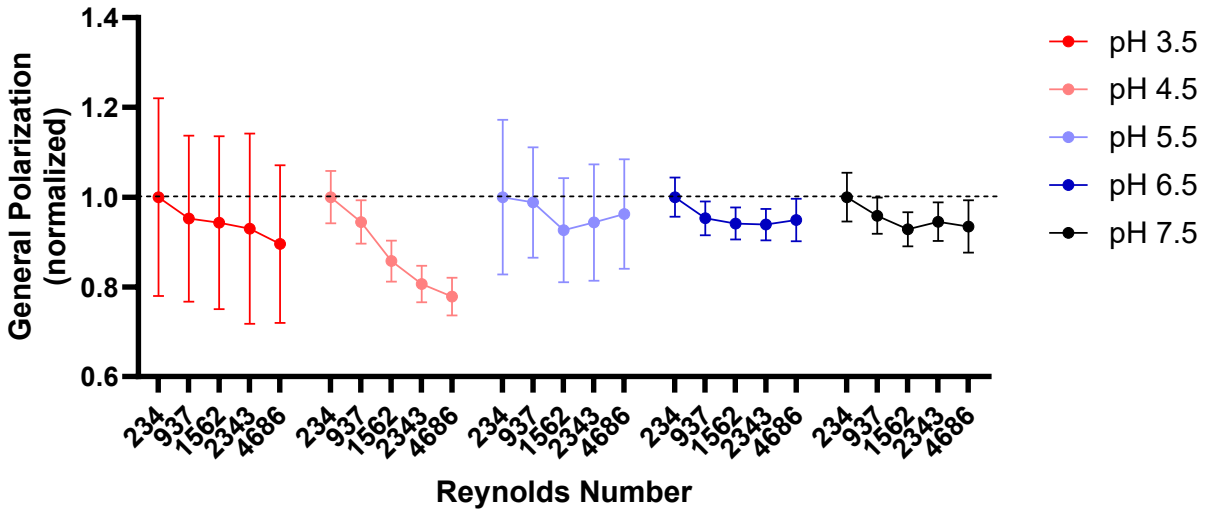

Supplemental Figure 4. Comparisons of general polarization (GP) via Laurdan assay at different pH, normalized to the lowest Re sample. GP is lower for every sample at every pH compared to the lowest Re sample, and usually trends down with higher Re, but the trend is most pronounced at pH 4.5.

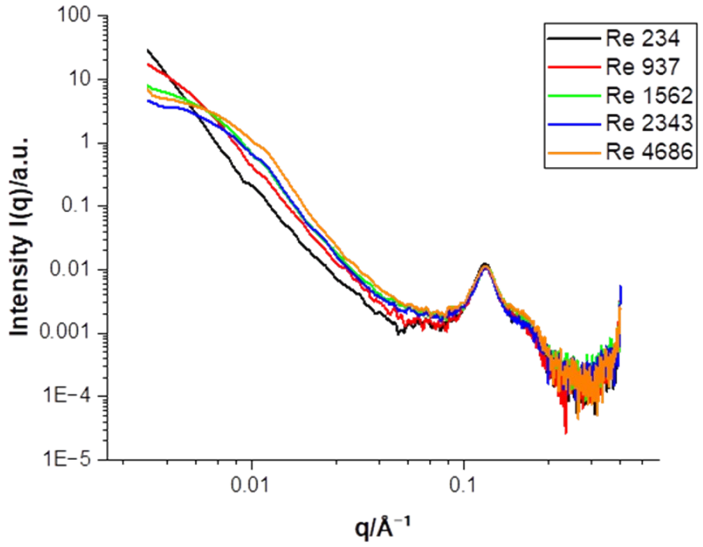

Supplemental Figure 5. Representative SAXS profiles in 10% trehalose for OF-02 LNPs made at different Re. Ordered structure was generally observed in all the samples approximately between 0.10 < q < 0.20 Å−1; however, differences were observed in this region depending on Re with respect to pH.

Reynolds Number	D_h (nm)	R_g (nm)
234	184	75
937	115	45
1562	91	31
2343	83	26
4686	79	26

Supplemental Table 3. Differences in hydrodynamic radius (R_h) and radius of gyration (R_g) versus Reynolds number (Re), as determined by Guinier analysis of the SAXS data in the low-q region. These same patterns are consistent with the DLS data.

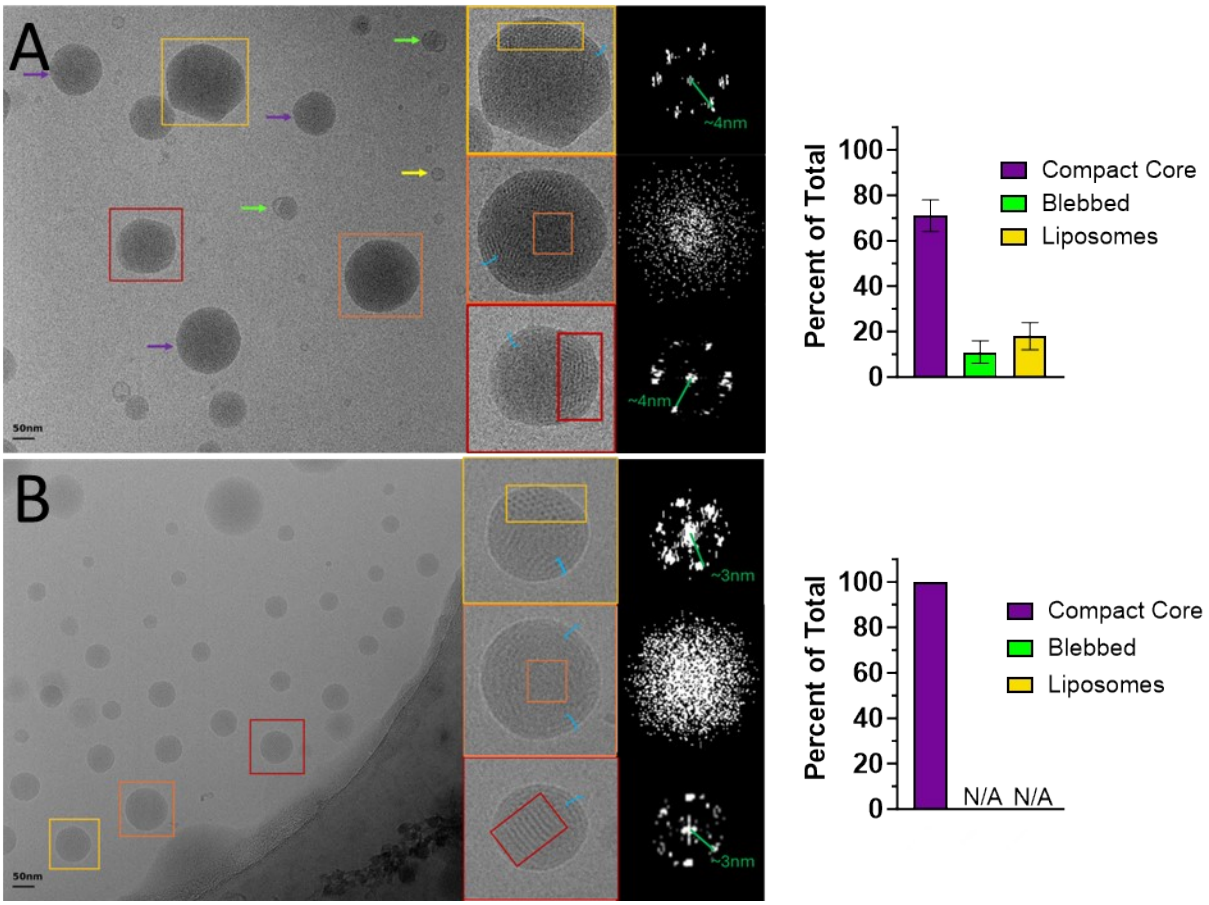

Supplemental Figure 6. Cryo-TEM images reveal distinct populations of particles in OF-02 LNPs made at high *versus* low Re. (A) Representative image of OF-02 LNPs made at Re = 234, illustrating structural heterogeneity. Three distinct structures are observed: compact core (purple arrows), blebs (green arrow), and lipid vesicles (yellow arrow). (B) Representative image of OF-02 LNPs made at Re = 4686. In both panels, the three boxed regions highlight representative LNPs with distinct internal lipid organizations. The first columns display magnified views of the boxed LNPs, while the second columns show the corresponding Fast Fourier Transforms (FFTs) of the selected areas. The yellow regions in the top cells reveal a crystalline hexagonal phase with a periodicity of approximately 3 or 4 nm (Re=4686 and Re=234 respectively), as indicated by the FFT. The orange regions in the middle cell correspond to an amorphous lipid arrangement, evidenced by the absence of defined peaks in the FFT. The red regions in the bottom cell display an inverse hexagonal phase with a periodicity of approximately 3 or 4 nm (Re=4686 and Re=234 respectively), as shown by the FFT pattern. In all zoomed-in views, a multilamellar region (highlighted by cyan brackets) is also visible.

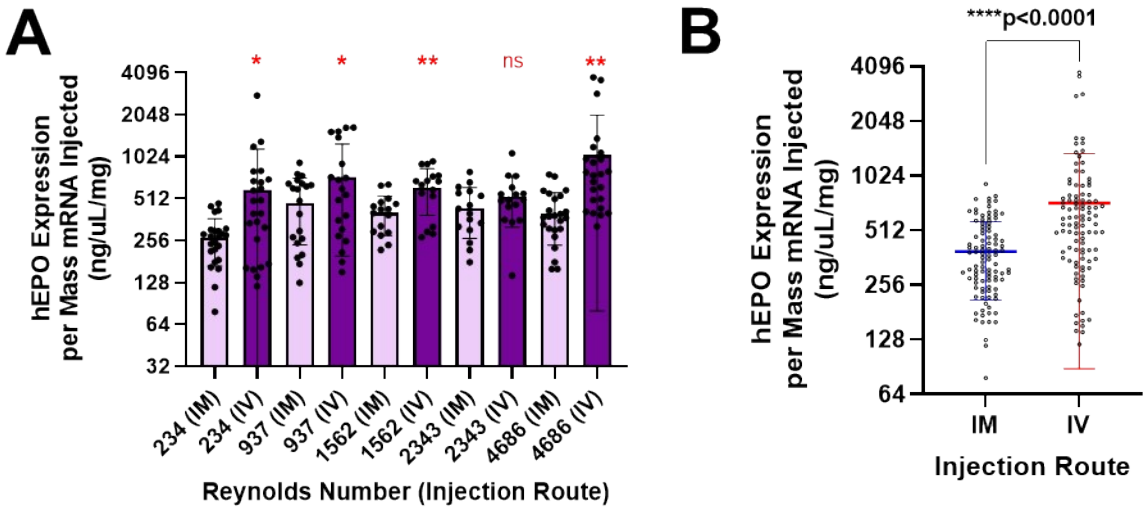

Supplemental Figure 7. Comparison of I.M. and I.V. routes of administration for OF-02 LNPs. (A) I.V. expression was generally higher per mass mRNA injected versus I.M. across a range of Re. (B) Scatterplot of all data points (irrespective of Re) demonstrates that expression is higher per mass of mRNA injected when LNPs are administered I.V. versus I.M. *$p < 0.10$, **$p < 0.01$, ns = not significant.